Research and Reviews in Materials Science and Chemistry
Vol. 5, Issue 1, 2015, Pages 1-27
ISSN 2319-6920
Published Online on July 31, 2015

http://jyotiacademicpress.net

SYNTHESIS AND CHARACTERIZATION OF SOME METAL COMPLEXES WITH A LIGAND DERIVED FROM NOVEL 1,2,3-TRIAZOLE DERIVATIVE AND EVALUATION OF THEIR ANTICANCER ACTIVITIES AND THE PERCENT OF uPA INHIBITION IN VITRO

NABIL S. YOUSSEF[1], SAYED A. DRWEESH[1], EMAN A. M. EL-ZAHANY[1], MAMDOUH M. ALI[2] and BAKR F. ABDEL-WAHAB[3]

[1]Department of Inorganic Chemistry
National Research Centre
P.O. Box 12622
Dokki, Giza
Egypt
e-mail: nabilyoussef@hotmail.com

[2]Department of Biochemistry
Division of Genetic Engineering and Biotechnology
National Research Center
P.O. Box 12622
Dokki, Giza
Egypt

[3]Department of Applied Organic Chemistry
National Research Centre
P.O. Box 12622
Dokki, Giza
Egypt

Keywords and phrases: 1,2,3-triazole, metal complexes, antiproliferative and human cancer cell lines.

Communicated by Ana Rosa Silva.

Received December 24, 2014; Revised June 12, 2015

Abstract

A new ligand, 2-(5-methyl-1-p-tolyl-1H-1,2,3-triazole-4-carbonyl)-N-phenylhydrazine-arbothioamide (H_3L) and its structure has been confirmed by elemental analysis, IR, mass, and NMR spectra. Mass spectra is also used to confirm the proposed formula and the possible fragments resulted from fragmentation of H_3L ligand. Its Co(II), Ni(II), Cu(II), Zn(II), Mn(II), Fe(III), and Ag(I) complexes have been prepared, characterized and their structures have been verified on the basis of analytical data, molar conductance, IR, NMR, UV-vis and magnetic measurements. The molar conductance data reveal that all complexes are non-electrolytes, except complexes 4 and 5 are ionic in nature. IR spectra show that H_3L ligand is coordinated to the metal ions in a tridentate manner with ONS atoms or tetradentate through ONS atoms beside the 1,2,3-triazole ring–N. The geometrical structures of these complexes are octahedral. The biological activities of H_3L ligand and its complexes have been tested in vitro, where cytotoxicity activity and the percent of Urokinase plasminogen activator (uPA) inhibition of them against three different human tumor cell lines including breast cancer cell line MCF-7, liver cancer cell line HepG2, and lung carcinoma A549 that may act through uPA inhibition were evaluated. The results showed that the metal complexes are more anticancer activity than the free ligand. This may be due to coordination and chelating trends to make metal complexes act as more powerful and potent anticancer agents, thus inhibiting the growth of the uPA. The Zn(II) complex (8) has the best complex exerting a significant cytotoxic compared to doxorubicin (the commonly used anticancer drug).

1. Introduction

Triazoles and their derivatives occupy a central position in modern heterocyclic chemistry due to their biologically active nature [1]. 1,2,3-Triazoles have occupied an important role not only in organic chemistry but also in medicinal chemistry due to their easy synthesis by click chemistry and attractive features as well as numerous biological activities. 1,2,3-Triazoles are highly stable under basic and acid hydrolysis and reductive oxidative conditions indicative of a high aromatic stabilization [2, 3]. Moreover, triazoles are an important class of heterocycles which, has a high dipole moment and is capable of hydrogen bonding, which could be favorable in the binding of biomolecular targets [4]. 1,2,3-Triazole is one of the key structural units found in a large variety of bioactive molecules as anti-fungal [5], antibacterial [6], anti-allergic [7], anti-HIV [8], anti-tubercular [9], anti-inflammatory agents [10], and antitumor [11].

Metal complexes with extended aromatic ligands can bind to DNA in a non-covalent fashion, especially through intercalative or groove binding [12]. Many studies suggest that DNA is the primary intracellular target of antitumor drugs, because the interaction between small molecules and DNA can cause DNA damage in cancer cells [13]. The design and synthesized metal based DNA probes is the most promising research area for the development of new therapeutic agents and tools in biochemistry its key role of DNA in cell life [14].

Cancer, the uncontrolled, rapid and pathological proliferation of abnormal cells, is one of the most formidable afflictions in the world. It is also a multifactor disease with superfluous and robust biological networks. It may require treatment with compounds that could target multiple intracellular components. Currently, cancer therapy interfering with a single biological molecule or pathway has been successfully utilized for the treatment in clinics [15, 16].

Urokinase plasminogen activator (uPA) is a serine protease that functions in the conversion of the circulating plasminogen to the active, broad-spectrum, serine protease plasmin. uPA is secreted as an inactive single-chain proenzyme by many different cell types and exists in a soluble or cell-associated form by binding to a specific membrane uPA receptor (uPAR) [17, 18]. The uPA is involved in many physiological functions and, along with members of the matrix metalloproteinases (MMPs) family; it has been implicated in cancer invasion and metastatization [19, 20, 21]. Besides the proteolytic function, upon binding to uPAR, uPA is involved in initiating versatile intracellular signal pathways that regulate cell proliferation, adhesion, and migration through its interaction with various integrins and vitronectin [22]. Urokinase is implicated in a large number of malignancies, e.g., cancers of breast, lung, bladder, cervix, kidney, stomach, and brain [23, 24]. The role of uPA in human cancer progression is further supported by clinical evidences demonstrating that high tissue levels of its components correlate with a poor prognosis in different types of cancer as breast, gastrointestinal cancers [25, 26]. In continuation to our investigations [27], a number of newly prepared biologically active triazole complexes with anticancer activity have been studied.

2. Experimental

2.1. Materials

All the reagents employed for the preparation of the ligands and their complexes were of the best grade available and used without further purification. They include hydrazine hydrate $NH_2NH_2 \cdot H_2O$, phenyl isothiocyante Ph-N = C = S, silver(I) nitrate $AgNO_3$, copper(II) sulphate pentahydrate $CuSO_4 \cdot 5H_2O$, nickel(II) sulphate hexahydrate $NiSO_4 \cdot 6H_2O$, nickel(II) chloride hexahydrate $NiCl_2 \cdot 6H_2O$, ferric(III) chloride $FeCl_3$, cobalt(II) chloride hexahydrate $CoCl_2 \cdot 6H_2O$, zinc acetate dehydrate $Zn(CH_3COO)_2 \cdot 2H_2O$, manganese(II) acetate tetrahydrate $Mn(CH_3COO)_2 \cdot 4H_2O$.

2.2. Physical measurements

The H_3L ligand and its metal complexes were analyzed for C, H, N, and metal contents at the Micro Analytical Laboratory, Faculty of Science, Cairo University, Egypt. Analytical and physical data of the ligand and its metal complexes are reported in Table 1. The metal ion contents of the complexes were also determined by the previously reported methods [28, 29]. IR spectra of the ligands and their metal complexes were measured using KBr discs with a Jasco FT/IR 300E Fourier transform infrared spectrophotometer covering the range $400cm^{-1}$-$4000cm^{-1}$, at the Central Laboratory, National Research Centre (NRC), Dokki, Egypt. The electronic spectra of the ligand and its complexes were obtained in Nujol mulls using a Shimadzu UV-240 UV-Vis recording spectrophotometer at the central laboratory, NRC, Dokki, Egypt. ^1H and ^{13}C NMR spectra were obtained on JöEL 500MHz spectrometer (Micro-analytical Unit, NRC). Chemical shifts (ppm) are reported relative to TMS. Molar conductivities of the metal complexes in DMSO $(10^{-3}M)$ were measured by using a dip cell and a Bibby conductimeter MC1 at room temperature. The resistance measured in ohms and the molar conductivities were calculated according to the equation: $\Lambda = V \times K \times Mw/g \times \Omega$, where Λ, molar conductivity $(ohm^{-1}$

$cm^2\ mol^{-1}$); V, volume of the complex solution (mL); K, cell constant $0.92cm^{-1}$; Mw, molecular weight of the complex; g, weight of the complex; and Ω, resistance measured in ohms. Magnetic susceptibilities were measured at 25ºC by the Gouy method using mercuric tetrathiocyanatocobaltate(II) as the magnetic susceptibility standard. Diamagnetic corrections were estimated from Pascal's constant [30]. The magnetic moments were calculated from the equation: $\mu_{eff.} = 2.84\sqrt{\chi_M^{corr}.T}$. Mass spectra of the ligand in the solid form was recorded by using JEUL JMS-AX-500 mass spectrometer.

2.3. Synthesis of the H_3L ligand

Ethyl 5-methyl-1-p-tolyl-1H-1,2,3-triazole-4-carboxylate **(1)** was prepared according to the reported procedure [31]. The 5-methyl-1-p-tolyl-1H-1,2,3-triazole-4-carbohydrazide **(2)** prepared by reaction of **1** (2.45g, 10mmol) with hydrazine hydrate (1.0g, 20mmol) in absolute ethanol (50mL), then the reaction mixture was boiled under reflux for 4h and cooled to room temperature. The precipitate was filtered off and recrystallized from ethanol, giving 70% of **2**. A mixture of **2** (1.12g, 5mmol) and phenylisothiocyante (0.67g, 5mmol) in absolute ethanol (30mL) was heated under reflux for 3h. The formed solid was filtered off and recrystallized from EtOH/DMF to give 2-(5-methyl-1-p-tolyl-1H-1,2,3-triazole-4-carbonyl)-N-phenylhydrazinecarbothioamide **(3)** in 65% yield, Scheme 1.

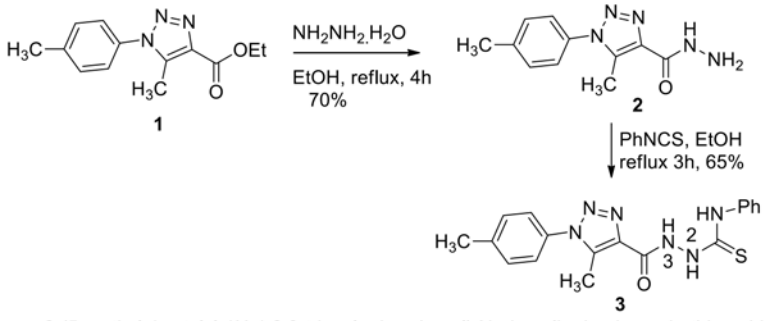

Scheme 1. Schematic representation for the formation of the H_3L ligand.

2.4. Synthesis of the metal complexes

The metal complexes of the H_3L ligand were prepared by dissolving the required amount of the H_3L ligand in mixture of MeOH/DMF (30/20ml), and then mixing with the methanol solution of the required amount of the metal salt to form 1:1 or 1:2 M/L (metal/ligand) complexes. The reaction mixture was then refluxed for a time depending on the transition metal salt used. The precipitates formed were filtered off, washed with methanol, then with diethyl ether and dried under vacuum at 50°C for 5h. The analytical data for the H_3L and its complexes are given in Table 1.

2.5. Biological evaluation

2.5.1. Chemicals

Fetal bovine serum (FBS) and L-glutamine, were obtained from Gibco Invitrogen Company (Scotland, UK). Dulbecco's modified Eagle's (DMEM) medium was provided from Cambrex (New Jersey, USA). Dimethyl sulfoxide (DMSO), doxorubicin, penicillin, and streptomycin were obtained from Sigma Chemical Company (Saint Louis, MO, USA). The level of uPA protein was determined by using Assay Max human urokinase (uPA) ELISA kit (Assaypro, USA).

2.5.2. Cell lines and culturing

Anticancer activity screening for the tested compounds utilizing 3 different human tumor cell lines including breast cancer cell line MCF-7, liver cancer cell line HepG2, and lung carcinoma cell line A549 were obtained from the American Type Culture Collection (Rockville, MD, USA). The tumor cells were maintained in Dulbecco's modified Eagle's medium (DMEM) supplemented with 10% heat inactivated fetal calf serum (GIBCO), penicillin (100U/ml) and streptomycin (100μg/ml) at 37°C in humidified atmosphere containing 5% CO_2. Cells at a concentration of 0.50×106, were grown in a $25cm^2$ flask in 5ml of complete culture medium.

2.5.3. In vitro cytotoxicity assay

The cytotoxicity was measured in vitro using the Sulfo-Rhodamine-B stain (SRB) assay according to the previous reported standard procedure [32]. Cells were inoculated in 96-well microtiter plate (104 cells/well) for 24h before treatment with the tested compounds to allow attachment of cell to the wall of the plate. Test compounds were dissolved in DMSO at 1mg/ml immediately before use and diluted to the appropriate volume just before addition to the cell culture. Different concentration of tested compounds and doxorubicin were added to the cells. Triplicate wells were prepared for each individual dose. Monolayer cells were incubated with the compounds for 48h at 37ºC and in atmosphere of 5% CO_2. After 48h cells were fixed, washed, and stained for 30 min with 0.4% (w/v) SRB dissolved in 1% acetic acid. Unbound dye was removed by four washes with 1% acetic acid, and attached stain was recovered with Tris-EDTA buffer. Colour intensity was measured in an ELISA reader. The relation between surviving fraction and drug concentration is plotted to get the survival curve for each cell line after the specified time. The concentration required for 50% inhibition of cell viability (IC50) was calculated and the results are given in Table 4. The results were compared to the antiproliferative effects of the reference control doxorubicin [33].

2.5.4. Determination the level of uPA protein expression

The level of uPA protein expression was determined by using Assay Max human urokinase (uPA) ELISA kit (Assaypro, USA) according to manufacturer's instructions. The prepared compounds as well as standard drug, doxorubicin were incubated for 48h with MCF7, HepG2 and A549 cells at concentration of 1/10 of the IC50 values of each compound which shown in Table 4. After 48h from compounds treatment, the medium was collected and centrifuged at 2000xg for 10 min to remove cellular debris. Add 50µl of the cell extract per well and incubate for 2h. Wells were washed with 200µl of wash buffer then add 50µl of biotinylated uPA antibody to each well and incubate for 1h at 25ºC. After washing, plates were incubated with 50µl of streptavidin-peroxidase

conjugate per well and incubate for 30 minutes then wash the microplate as described above. Add 50µl of chromogen substrate per well and incubate for about 10 min or till the optimal blue colour density develops. Add 50µl of stop solution to each well. The colour will change from blue to yellow. Read the absorbance on a microplate reader at a wavelength of 450nm immediately and the concentrations of uPA in the samples were determined.

2.5.5. Statistical analysis

The results are reported as Mean ± Standard error (S.E.) for at least three times experiments. Statistical differences were analyzed according to followed by one way ANOVA test followed by student's test wherein the differences were considered to be significant at $p < 0.05$.

3. Results and Discussion

3.1. Elemental analysis

The elemental and physical data of the ligand H_3L and its complexes (Table 1) showed that the stoichiometry of the complexes obtained is either 1:1 or 1:2 M/L.

3.2. Mass spectra of the ligand

The mass spectra of the ligand H_3L revealed the molecular ion peaks at m/e 366, which is coincident with the formulae weights 366.44, for this ligand and supports the identity of their structures. The pathway fragmentation pattern of the mass spectra of this ligand is depicted in Scheme 2.

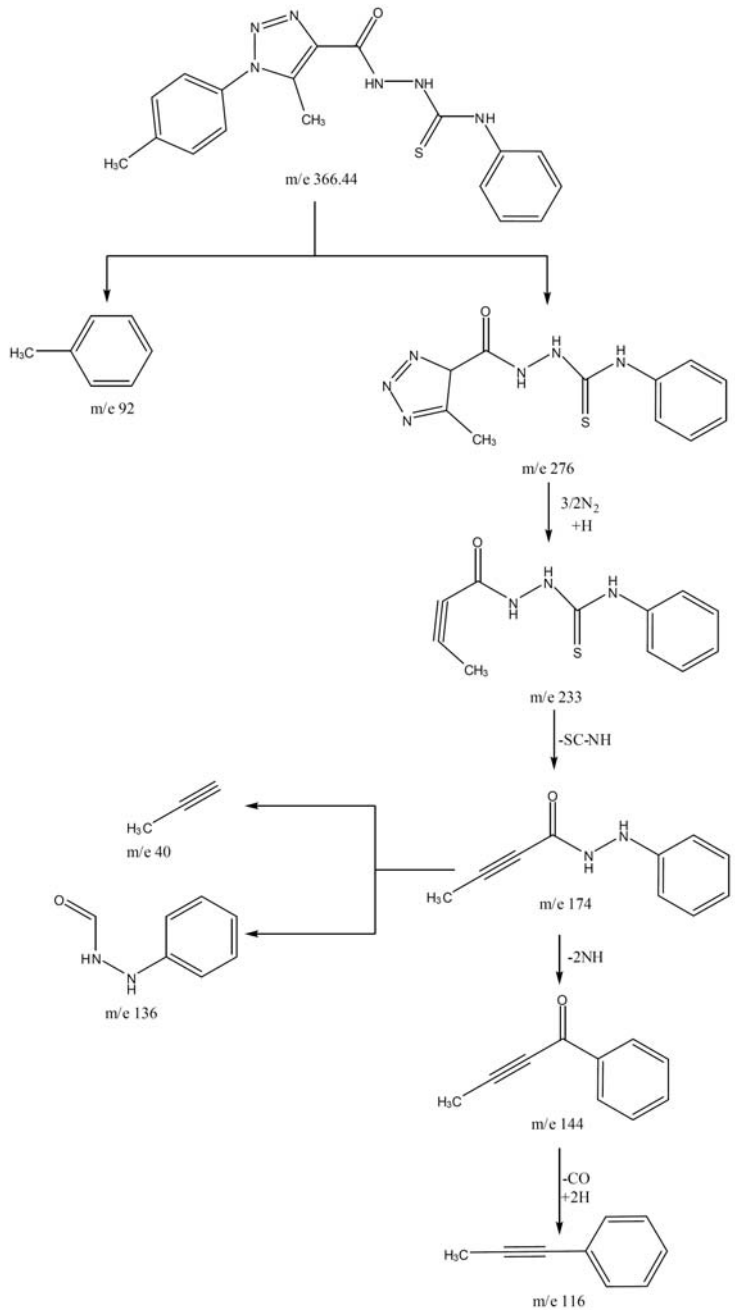

Scheme 2. The pathway fragmentation pattern of the mass spectrum of the ligand H_3L.

3.3. Conductivity measurements

All metal complexes are stable in air and soluble in DMSO. The molar conductivity of the complexes in DMSO at the concentration 10^{-3}M in the range $(10 - 92)\Omega^{-1}cm^2mol^{-1}$ are listed in Table 1. All complexes showed a non-electrolyte nature [34, 35] except 4, 5, and 9 complexes behaved as electrolytes [36].

Table 1. Analytical and physical data of the ligand H_3L and its metal complexes

No.	Ligands/complexes	Colour	FW	Yield (%)	Anal./found (calc.) (%)					Molar conductance $\Lambda m(\Omega^{-1}cm^2mol^{-1})$
					C	H	N	S	M	
1	H_3L, $C_{18}H_{18}N_6OS$	colourless	366.44	65	58.9 (59.5)	4.9 (5.4)	22.9 (23.3)	8.7 (9.2)	–	–
2	$[HLCo(H_2O)_2]\cdot 2(H_2O)$ $C_{18}H_{24}CoN_6O_5S$	brown	495.42	70	43.6 (44.0)	4.8 (4.5)	16.9 (16.5)	6.4 (5.9)	11.9 (12.4)	12
3	$[HLCu(H_2O)_2]\cdot (H_2O)$ $C_{18}H_{22}CuN_6O_4S$	grey	482.02	75	44.8 (45.3)	4.6 (4.9)	17.4 (17.9)	6.6 (6.9)	13.1 (13.5)	10
4	$[H_3LAg(H_2O)_2]\cdot NO_3(H_2O)$ $C_{18}H_{24}AgN_7O_7S$	brown	590.36	72	36.6 (37.0)	4.1 (4.6)	16.6 (16.2)	5.4 (4.9)	18.2 (17.7)	79
5	$[H_3LNi\cdot (H_2O)_2]\cdot Cl_2$ $C_{18}H_{22}Cl_2N_6NiO_3S$	green	532.07	66	40.6 (41.1)	4.1 (4.6)	15.7 (15.2)	6.0 (5.7)	11.0 (10.8)	68
6	$[H_3LFeCl_3]\cdot (H_2O)$ $C_{18}H_{20}Cl_3FeN_6O_2S$	brown	546.66	78	39.5 (39.0)	3.6 (4.0)	15.3 (15.8)	5.8 (5.4)	10.2 (9.7)	11
7	$[(H_2L)_2Ni]\cdot 3(H_2O)$ $C_{36}H_{42}N_{12}NiO_5S_2$	grey	845.62	65	51.1 (50.8)	5.0 (5.3)	19.8 (20.2)	7.5 (7.9)	6.9 (6.7)	12
8	$HLZn(H_2O)_2$ $C_{18}H_{20}N_6O_3SZn$	yellow	465.84	73	46.4 (47.0)	4.3 (4.8)	18.0 (18.4)	6.8 (7.2)	14.0 (13.5)	13
9	$[(H_3L)_2Mn]\cdot 2(OCOCH_3)$ $C_{40}H_{42}MnN_{12}O_6S_2$	yellow	905.91	70	53.0 (52.7)	4.6 (5.0)	18.5 (18.1)	7.0 (6.5)	6.0 (5.6)	92

3.4. Infrared spectra

The significant IR bands of the ligand and its metal complexes are given in Table 2. The ligand H_3L can exhibit tautomerism, since it contains NH-C=S and NH-C=O functional groups, respectively. However, the absence of the ν (S-H) band at $2570cm^{-1}$ or a band at higher than $3500cm^{-1}$ due to hydroxyl form of the enolic structure in the spectrum of ligand H_3L indicates the thionic and ketonic nature of this ligand in the solid state [37, 38]. The IR spectrum of ligand H_3L displays two bands at $3244cm^{-1}$ and $3120cm^{-1}$ arising from two –NH groups attached to –C=O and –C=S groups, respectively, present in the ligand. Moreover, the peaks shown at 1655, 1496, 1232, (1074-1008), $716cm^{-1}$ are assigned to amide I, thioamide I, (N=N) triazole ring, (N-N), and ν(C=S), respectively. The modes of coordination of the complexes were made by comparison with the vibrational frequencies of the free ligand.

Table 2. IR frequencies of the bands (cm^{-1}) of ligand H_3L and its metal complexes and their assignments

No.	Ligand/complex	ν (NH –C=O)	ν (NH–C=S)	Amide 1 ν(C=O)	ν (C=S)	Thio amide 1	ν (N=N–N–N) triazole ring	ν_s(Coo), ν_{as}(Coo)/ NO_3	$(N_2 - N_3)$	$\nu(H_2O + NH)$
1	H_3L	3237	3136	1655	719	1496	1232 1074	–	1008	–
2	$[HLCo(H_2O)_2] \cdot 2(H_2O)$	–	–	–	755 693	1458	1292 1088	–	1035	3415
3	$[HLCu(H_2O)_2] \cdot (H_2O)$	–	–	–	696	1451	1293 1164	–	1040	3418
4	$[H_3LAg(H_2O)_2] \cdot NO_3(H_2O)$	3250	3197	1566	696	1419	1290 1148	821	1039	3434
5	$[H_3LNi \cdot (H_2O)_2] \cdot Cl_2$	3242	3146	1623	701	1439	1261 1124	–	1048	3491
6	$[H_3LFeCl_3] \cdot (H_2O)$	3232	3135	1598w	696	1451	1284 1192	–	1014	3425
7	$[(H_2L)_2Ni] \cdot 3(H_2O)$	3242	–	1622	700	1439	1234 1178	–	1013	3440
8	$HLZn(H_2O)_2$	–	–	–	698	1455	–	–	1017	3420
9	$[(H_3L)_2Mn] \cdot 2(OCOCH_3)$	–	–	–	698	1455	1237 1075	1538 1381	1036	3440

The IR data obtained suggested that the ligand behaves as a tetradentate ligand and coordinates through the amide I, (N=N) of the triazole ring, hydrazinic nitrogen and ν(C = S), respectively, in case of complexes (2-5) and 8. In these complexes, the mode of coordination was suggested by the following evidences: (i) the shift of (N=N) triazole ring and hydrazinic nitrogen bands at higher wave numbers; (ii) the shift and weakness of C=O and C=S bands in complexes 4 and 5 which indicate the involvement of the ketone oxygen and thione sulphur on complexation; and (iii) disappearance of the two bands due to ν(NH) adjacent to the thione sulphur and NH adjacent to C=O in complexes 2, 3, and 8 that suggests the loss of a proton via keto-enol tautomerism and participation of the deprotonated hydrazinic nitrogen and C−O group on complex formation.

The ligand behaves as a tridentate in the complexes 6, 7, and 9 and coordinates through the amide I, hydrazinic nitrogen, and ν(C=S), respectively. In these complexes, the mode of coordination was suggested by the following evidences: (i) the occurrence of the ν(NN) band at higher wave numbers; (ii) the shift and weakness of C=O and C=S bands in these complexes which indicate involvement of the ketonic and thionic groups of the ligand on complexation; and (iii) disappearance of the two bands due to (NH) adjacent to NH-C=S and NH-C=O in complexes 7 and 8 which suggests loss of a proton after keto-enol tautomerism followed by participation of the deprotonated hydrazinic nitrogen and C−O group on complexation.

The appearance of two characteristic bands at 1538 and 1381cm^{-1} in case of complex 9 was attributed to ν_{as}(O–C–O), and ν_s(O–C–O) of the acetate group with a difference in wave number less than 164cm^{-1} indicating the participation of the carboxylate oxygen on complex formation in ionic fashion [39].

The appearance of a new band at 821cm^{-1} in case of complex 4 may be attributed to NO_3 group in an ionic fashion [40].

3.5. NMR studies

The ^{1}H NMR spectrum of H_3L exhibits signals at 9.76 and 10.58ppm for the amide –NH(CO) and thioamide –NH(CS) protons, respectively. The ^{13}C NMR spectrum of H_3L shows signals at 181.62, 160.42ppm due to the C=S and C=O carbons, respectively. The expected structure of H_3L is shown in Figure 1. Actually, all the studied metal complexes were almost insoluble in most organic solvents, and a good solubility was observed only in DMSO and DMF. Unfortunately, any attempt to grow crystals suitable for X-ray structural determination from these solvents met with failure. When we tried to record NMR spectra in deuterated DMSO, we observed broad signals that prevented any attribution of the chemical shifts. The only complex that showed a good solubility even in chlorinated solvents was complex 4. In this case, it was possible to record a ^{1}H NMR spectrum in $CDCl_3$, that is in agreement with a diamagnetic complex. The ^{1}H NMR spectra of the silver complex in DMSO-d^6 was interpreted by comparing its spectra with that of H_3L. The ^{1}H NMR spectra of Ag(I) complex shows shifting of the two signals of the amide –NH(CO) and thioamide –NH(CS) protons, respectively, to at 10.50ppm and 10.99ppm. The presence of the signal due to the hydrazinic proton indicates complex formation without deprotonation.

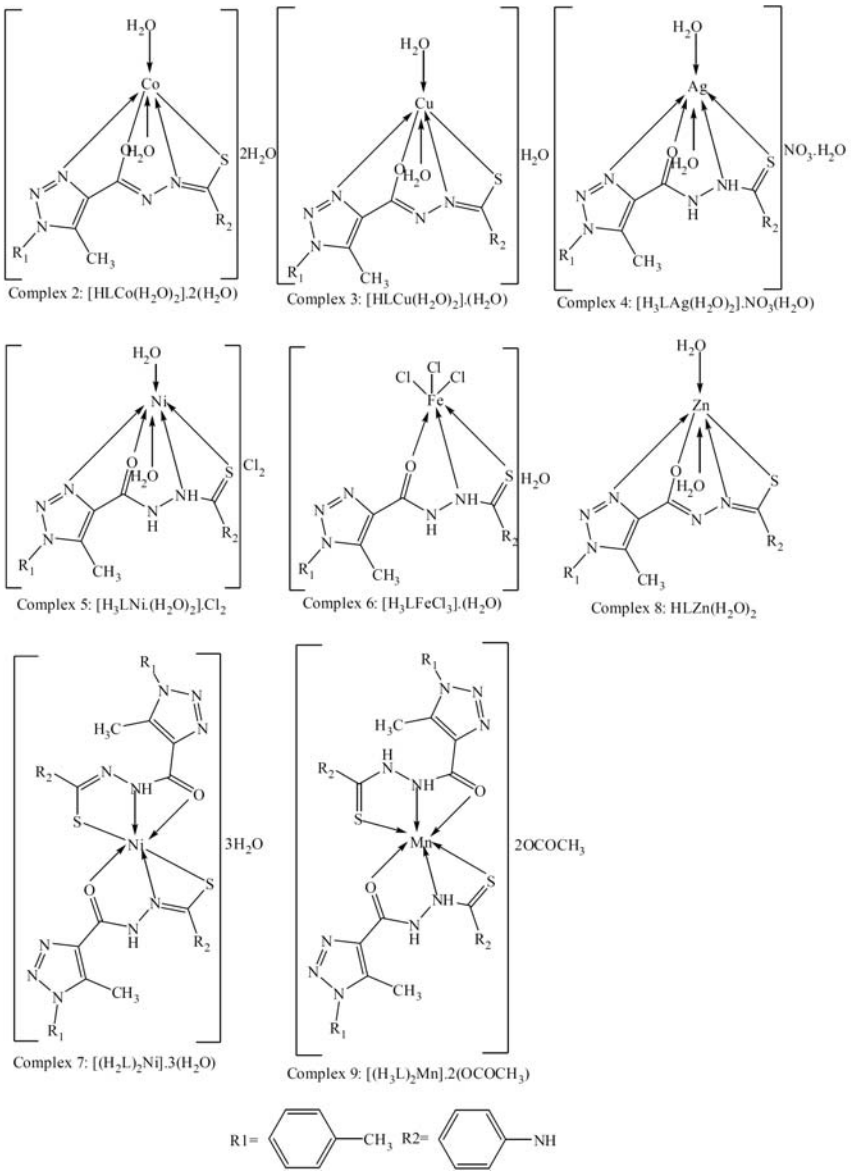

Figure 1. Structural formulae of H_3L metal complexes.

3.6. Electronic spectra and magnetic moments

The electronic spectra of the H_3L ligand and its complexes (1-9) have been recorded in the 200-1000nm range as shown in Table 3. Upon complexation with metal ions, the absorption bands attributed to $\pi \rightarrow \pi^*$ and $n \rightarrow \pi^*$ transitions were found to be shifted to lower or higher energy regions compared to the free ligand. In addition, the appearance of new bands at longer wavelengths may be assigned to LMCT/d–d transitions. The electronic spectra of the H_3L complexes showed that strong charge transfer transitions interfere and prevent the observation of all the expected d-d bands. The broad band at approximately 425-455nm is assignable to a combination of phenoxy $O \rightarrow M$ transition, imine $N \rightarrow M$(II, or III), CT($L(\pi) \rightarrow$ MCT), and M(II, III) d-d bands. This generally confirms that the ligand interacts with the metal ions, and the metal ions environments are different leading to the formation of different geometrical types of complexes. Figure 2 shows the electronic spectra of Co(II), Cu(II), and Fe(III) complexes, as representative examples.

Table 3. The electronic absorption spectral bands (nm) and magnetic moment (B.M) for the ligands H_3L and its complexes

No.	Ligand/complex	λ_{max}(nm)		Geometry	μ_{eff} in BM
		Ligand and CT bands	d-d bands		
1	H_3L	300, 317, 333	–	–	–
2	$[HLCo(H_2O)_2]\cdot 2(H_2O)$	317, 400, 415	547, 730	octahedral	5.10
3	$[HLCu(H_2O)_2]\cdot (H_2O)$	315, 382	506, 680	distorted octahedral	1.92
4	$[H_3LAg(H_2O)_2]\cdot NO_3(H_2O)$	315, 430	–	octahedral	–
5	$[H_3LNi\cdot (H_2O)_2]\cdot Cl_2$	292, 336	450	octahedral	3.10
6	$[H_3LFeCl_3]\cdot (H_2O)$	317, 401, 426	581, 732, 845	octahedral	5.65
7	$[(H_2L)_2Ni]\cdot 3(H_2O)$	318, 393	656, 980	octahedral	3.50
8	$HLZn(H_2O)_2$	315, 367	–	octahedral	–
9	$[(H_3L)_2Mn]\cdot 2(OCOCH_3)$	290, 315, 390	545	octahedral	5.85

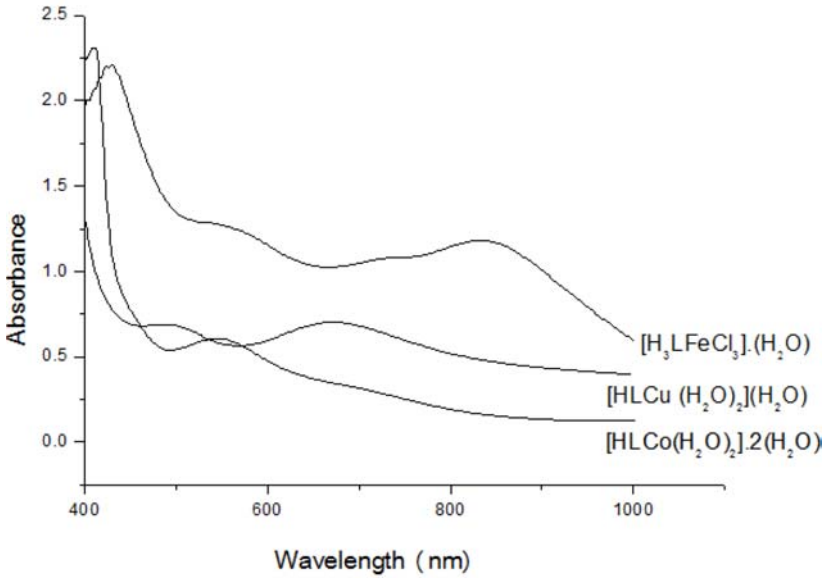

Figure 2. UV spectra of some H_3L complexes.

The metal ion, Co(II) (d^7) gives rise to the free ion terms 4F, 4P and a number of doublet states. The electronic spectra of Co(II) complex (2) displays three bands at 730nm, 547nm, and 415nm, respectively, assignable to the transitions $^4T_1g(F) \rightarrow {}^4T_2g(F)(\upsilon_1)$, $^4T_1g(F) \rightarrow {}^4A_2g(F)(\upsilon_2)$, and $^4T_1g(F) \rightarrow {}^4T_1g(P)(\upsilon_3)$, respectively, of the d^7-system suggesting Co(II) high-spin complex octahedral environment of donor atoms with a ground state term symbol ^4F. Its magnetic moment value (5.10BM) confirms the octahedral structure [41, 42].

The electronic spectrum of Fe(III) complex (6) exhibits bands at 845nm, 732nm, and 581nm which may be due to $^6A_1g \rightarrow {}^4T_1g(G)$, $^6A_1g \rightarrow {}^4T_2g(G)$, and $^6A_1g \rightarrow {}^4A_1g(G)$ transitions, respectively, suggesting its octahedral nature. The magnetic moment of this complex is 5.65BM, which is closer to the spin only value indicating an octahedral structure of the complex [41, 43, 44, 45, 46].

The electronic spectra of the Cu(II) complex (3) displays two bands at 680nm and 506nm assigned to $^2B_1g \rightarrow {}^2A_1g$ and $^2B_1g \rightarrow {}^2E_g$ transitions suggesting a distorted octahedral environment around Cu(II) ion as expected from the Jahn-Teller distortion in hexa-coordinated d^9 metal ion. The magnetic moment of copper complex is (1.92BM) indicates the presence of an unpaired electron on Cu(II) ion in an octahedral geometry environment [46, 47, 48].

Mn(II) complex (9) electronic spectrum displays weak absorption bands at 545nm characteristic of octahedral geometry. This band is assigned as $^6A_1g \rightarrow {}^4T_1g(4G)$ transition [49]. The magnetic moment of this Mn(II) complex is 5.85BM [50, 51] corresponding to high-spin configuration due to five unpaired electrons in ground state 6S (6A1) in which orbital contribution to the magnetic moment is quenched.

The broad band at 450nm in the spectra of Ni(II) complex (5) may be assigned to the $^3A_2g \rightarrow {}^3T_1g(F)$ transition, suggesting octahedral Ni(II) complex [52]. The electronic spectrum of Ni(II) complex (7) shows d–d transitions at 980nm and 656nm assigned to $^3A_2g(F) \rightarrow {}^3T_2g(F)$ (υ_1) and $^3A_2g(F) \rightarrow {}^3T_1g(F)$ (υ_2) spin allowed electronic transitions, which are characteristic of Ni(II) in an octahedral configuration [49]. The effective magnetic moment values of 3.10 and 3.50BM of the nickel complexes also indicate the octahedral structure of these complexes [53].

The Zn(II) and Ag(I) complexes 8 and 4, are diamagnetic as expected for d^{10} system, according to the elemental formulae and their spectral data, we proposed an octahedral geometry for these complexes [54].

3.7. Biological activities

3.7.1. In vitro cytotoxicity

As shown in Table 4, the cytotoxicity of the synthetic compounds was tested by using SRB assay as described by Skehan [32] in breast cancer cell line MCF-7, liver cancer cell line HepG2, and lung carcinoma cell line A549. For comparison, doxorubicin was also tested. The results revealed

that, in case of MCF-7, HepG2, and A549, the most active compound 8 exhibited higher activity (IC50 : 2.67 ± 0.27, 4.00 ± 0.41, and 3.70 ± 0.32μg/ml, respectively) than doxorubicin (IC50 : 2.98 ± 0.21, 4.20 ± 0.32, and 3.77 ± 0.34μg/ml, respectively). Also, the metal complexes are more anticancer activity than the free ligand; this may be due to the change in structure due to coordination and chelating trends to make metal complexes act as more powerful and potent anticancer agents, thus inhibiting the growth of the uPA. Moreover, This would suggest that the chelation could facilitate the ability of a complex to cross a cell membrane and can be explained by Tweedy's chelation theory chelation considerably reduces the polarity of the metal ion mainly because of partial sharing of its positive charge with the donor groups and possible electron delocalization over the whole chelate ring. Such chelation could also enhance the lipophilic character of the central metal atom, which subsequently favours its permeation through the lipid layer of the cell membrane [55]. Moreover, most of the synthetic intermediates were of moderately to strong cytotoxicity against the three cell lines. The order of activity of the compounds was 8, 7, 5, 2, 9, 3, 4, 6 and H_3L ligand in a descending order, with the exception in the lung carcinoma cell line A549. The H_3L ligand and its complexes 3, 6, and 9 showed no activity.

Table 4. In vitro cytotoxicity and the percent of uPA inhibition of the synthesized compounds on different cell lines

No.	Compound	IC_{50}(μg/ml)			% of uPA inhibition		
		MCF-7	HepG2	A549	MCF-7	HepG2	A549
	Doxorubicin	2.98 ± 0.21	4.20 ± 0.32	3.77 ± 0.34	86	84	81
	DMSO	N.A.	N.A.	N.A.	N.A.	N.A.	N.A.
1	H_3L	19.90 ± 1.71	22.60 ± 1.80	N.A.	3	N.A.	N.A.
2	$[HLCo(H_2O)_2] \cdot 2(H_2O)$	4.25 ± 0.23	5.36 ± 0.46	5.00 ± 0.42	73	68	60
3	$[HLCu(H_2O)_2] \cdot (H_2O)$	8.70 ± 0.46	10.24 ± 0.98	N.A.	16	12	N.A.
4	$[H_3LAg(H_2O)_2] \cdot NO_3(H_2O)$	18.20 ± 1.32	20.00 ± 1.78	13.80 ± 1.28	5	N.A.	4
5	$[H_3LNi \cdot (H_2O)_2] \cdot Cl_2$	3.95 ± 0.25	4.90 ± 0.34	4.90 ± 0.38	75	70	64
6	$[H_3LFeCl_3] \cdot (H_2O)$	18.70 ± 0.43	11.12 ± 0.67	N.A.	7	11	N.A.
7	$[(H_2L)_2Ni] \cdot 3(H_2O)$	3.82 ± 0.31	4.80 ± 0.38	4.80 ± 1.24	81	77	70
8	$HLZn(H_2O)_2$	2.67 ± 0.27	4.00 ± 0.41	3.70 ± 0.32	85	79	79
9	$[(H_3L)_2Mn] \cdot 2(OCOCH_3)$	4.85 ± 0.35	5.76 ± 0.47	N.A.	60	62	N.A.

Data were expressed as mean ± standard error (S.E.) of three independent experiments.

N.A. is no activity.

Conclusion

Metal complexes were prepared by the reaction of H_3L and transition metal ions such as Co(II), Ni(II), Cu(II), Zn(II), Mn(II), Fe(III), and Ag(I) in 1:1 or 1:2 M/L molar ratios and their structures were proposed from analytical and spectral data. The biological results suggest that the tested compounds could be used as alternative to synthetic chemotherapeutic agents. The results showed also that the metal complexes have more anticancer activity than the free ligand. This may be due to coordination and chelating to the ligand H_3L. The Zn(II) complex (8) is the best complex exerting a significant cytotoxic compared to doxorubicin (the commonly used anticancer drug).

References

[1] M. Hanif and Z. H. Chohan, Design, spectral characterization and biological studies of transition metal (II) complexes with triazole Schiff bases, Spectrochim Acta A Mol. Biomol. Spectrosc. 104 (2013), 468-476.

[2] N. S. Vatmurge, B. G. Hazra, V. S. Pore, F. Shirazi, P. S. Chavan and M. V. Deshpande, Synthesis and antimicrobial activity of beta-lactam-bile acid conjugates linked via triazole, Bioorg. Med. Chem. Lett. 18 (2008), 2043-2047.

[3] M. Whiting, J. Muldoon, Y. C. Lin, S. M. Silverman, W. Lindstron, A. J. Olson, H. C. Kolb, M. G. Finn, K. B. Sharpless, J. H. Elder and V. V. Fokin, Inhibitors of HIV-1 protease by using in situ click chemistry, Angew. Chem. Int. Ed. 45 (2006), 1435-1439.

[4] V. D. Bock, D. Speijer, H. Hiemstra and J. H. V. Maarseveen, 1,2,3-Triazoles as peptide bond isosteres: Synthesis and biological evaluation of cyclotetrapeptide mimics, Org. Biomol. Chem. 5 (2007), 971-976.

[5] N. G. Aher, V. S. Pore, N. N. Mishra, A. Kumar, P. K. Shukla, A. Sharma and M. K. Bhat, Synthesis and antifungal activity of 1,2,3-triazole containing fluconazole an alogues, Bioorg. Med. Chem. Lett. 19 (2009), 759-763.

[6] J. A. Demaray, J. E. Thuener, M. N. Dawson and S. J. Sucheck, Synthesis of triazoleoxazolidinones via a one-pot reaction and evaluation of their antimicrobial activity, Bioorg. Med. Chem. Lett. 18 (2008), 4868-4871.

[7] D. R. Buckle, D. J. Outred, C. J. M. Rockell, H. Smith and B. A. Spicer, Studies on ν-triazoles, 7. antiallergic 9-oxo-1H, 9H-benzopyrano [2,3-d]-ν-triazoles, J. Med. Chem. 26 (1983), 251-254.

[8] M. J. Giffin, H. Heaslet, A. Brik, Y. C. Lin, G. Cauvi, C. H. Wong, D. E. McRee, J. H. Elder, C. D. Stout and B. E. Torbett, A copper (I)-catalyzed 1,2,3-triazole azidealkyne click compound is a potent inhibitor of a multidrug-resistant HIV-1 protease variant, J. Med. Chem. 51 (2008), 6263-6270.

[9] S. R. Patpi, L. Pulipati, P. Yogeeswari, D. Sriram, N. Jain, B. Sridhar, R. Murthy, D. T. Anjana, S. V. Kalivendi and S. Kantevar, Design, synthesis, and structure activity correlations of novel dibenzo [b, d] furan, dibenzo [b, d] thiophene, and N-methylcarbazole clubbed 1,2,3-triazoles as potent inhibitors of mycobacterium tuberculosis, J. Med. Chem. 55 (2012), 3911-3922.

[10] R. D. Simone, M. G. Chini, I. Bruno, R. Riccio, D. Mueller, O. Werz and G. Bifulco, Structure-based discovery of inhibitors of microsomal prostaglandin E2 synthase-1,5-lipoxygenase and 5-lipoxygenase-activating protein: Promising hits for the development of new anti-inflammatory agents, J. Med. Chem. 54 (2011), 1565-1575.

[11] Y.-C. Duan, Y.-C. Ma, E. Zhang, X.-J. Shi, M.-M. Wang, X.-W. Ye and H.-M. Liu, Design and synthesis of novel 1,2,3-triazole-dithiocarbamate hybrids as potential anticancer agents, Eur. J. Med. Chem. 62 (2013), 11-19.

[12] L. H. Hurley, DNA and its associated processes as targets for cancer therapy, Nat. Rev. Cancer 2 (2002), 188-200.

[13] A. Nori and J. Kopeček, Intracellular targeting of polymer-bound drugs for cancer chemotherapy, Advanced Drug Delivery Reviews 57 (2005), 609-636.

[14] S. Poornima, S. Anbu, R. Ravishankaran, S. Sundaramoorthy, K. N. Vennila, A. A. Karande, D. Velmurugan and M. Kandaswamy, DNA and protein targeting 1,2,4-triazole based water soluble dinickel(II) complexes enhances antiproliferation and lactate dehydrogenase inhibition, Polyhedron 62 (2013), 26-36.

[15] P. Singh, R. Raj, V. Kumar, M. P. Mahajan, P. M. S. Bedi, T. Kaur and A. K. Saxena, 1,2,3-Triazole tethered β-lactam-Chalcone bifunctional hybrids: Synthesis and anticancer evaluation, Eur. J. Med. Chem. 47 (2012), 594-600.

[16] A. Petrelli and S. Giordano, From single- to multi-target drugs in cancer therapy: When aspecificity becomes an advantage, Curr. Med. Chem. 15 (2008), 422-432.

[17] M. J. Duffy, The urokinase plasminogen activator system: Role in malignancy, J. Curr. Pharm. Des. 10 (2004), 39-49.

[18] T. Syrovets and T. Simmet, Novel aspects and new roles for the serine protease plasmin, Cell Mol. Life Sci. 61 (2004), 873-885.

[19] M. J. Duffy, Urokinase plasminogen activator and malignancy, Fibrinolysis 7 (1993), 295-302.

[20] P. Mignatti and D. B. Rifkin, Biology and biochemistry of proteinases in tumor invasion, Physiol. Rev. 73 (1993), 161-195.

[21] K. Bdeir, A. Kuo, B. S. Sachais, A. H. Rux, Y. Bdeir, A. Mazar, A. A.-R. Higazi and D. B. Cines, The kringle stabilizes urokinase binding to the urokinase receptor, Blood 102 (2003), 3600-3608.

[22] F. Blasi and P. Carmeliet, uPAR: A versatile signalling orchestrator, Nat. Rev. Mol. Cell Biol. 3 (2002), 932-943.

[23] P. A. Andreasen, L. Kjoller, L. Christensen and M. J. Duffy, The urokinase-type plasminogen activator system in cancer metastasis: A review, Int. J. Cancer 72 (1997), 1-22.

[24] T. Meyer and I. Hart, Mechanisms of tumour metastasis, Eur. J. Cancer 34 (1998), 214-221.

[25] N. Sidenius and F. Blasi, The urokinase plasminogen activator system in cancer: Recent advances and implication for prognosis and therapy, Cancer Metastasis Rev. 22 (2003) 205-222.

[26] M. J. Duffy and C. Duggan, The urokinase plasminogen activator system: A rich source of tumour markers for the individualised management of patients with cancer, Clin Biochem. 37 (2004), 541-548.

[27] E. A. El-Zahany, M. M. Ali, S. A. Drweesh, A. M. A. El-Seidy, B. F. Abdel-Wahab and N. S. Youssef, Synthesis, characterization, and antiproliferative activity of Cu^{2+}, $V(IV)O^{2+}$, Co^{2+}, Mn^{2+}, and Ni^{2+} complexes with 3-(2-(4-methoxyphenylcarbamothioyl)hydrazinyl)-3-OXO-N-(thiazol-2-yl) propanamide against human breast adenocarcinoma cells, Phosphorus, Sulfur, and Silicon and the Related Elements 189 (2014), 762-777.

[28] A. I. Vogel, A Text Book of Quantitative Inorganic Analysis, 4th Edition, London: Longmans, 1978.

[29] Z. Holzbecher, L. Divis, M. Kral, L. Sucha and F. Vracil, Handbook of Organic Reagents in Inorganic Analysis, Chichester, Wiley, 1976.

[30] T. M. Salama, A. H. Ahmed and Z. M. El-Bahy, Y-type zeolite-encapsulated copper(II) salicylidene-*p*-aminobenzoic Schiff base complex: Synthesis, characterization and carbon monoxide adsorption, Microporous and Mesoporous Materials 89 (2006), 251-259.

[31] H.-S. Dong, G.-Y. Huo and Z.-T. Ma, The synthesis of some new (1-aryl-5-methyl-1H-1,2,3-triazol-4-yl) diarylmethanol, Indian J. Chem. 47(B) (2008), 171-174.

[32] P. Skehan, R. Storeng, D. Scudiero, A. Monks, J. Mahon, D. Vistica, J. T. Warren, H. Bokesch, S. Kenney and M. R. Boyd, New colorimetric cytotoxicity assay for anticancer-drug screening, J. Natil. Cancer Inst. 82 (1990), 1107-1112.

[33] L. Li, R. Qu, A. de Kochko, C. Fauquet and R. N. Beachy, An improved rice transformation method using the biolistic method, Plant Cell Rep. 12 (1993), 250-255.

[34] A. Golcu, M. Tumer, H. Demirelli and R. A. Wheatley, Cd(II) and Cu(II) complexes of polydentate Schiff base ligands: Synthesis, characterization, properties and biological activity, Inorg. Chim. Acta 358 (2005), 1785-1797.

[35] M. S. Refat, M. A. A. Moussa and S. F. Mohamed, Synthesis, spectroscopic characterization, thermal analysis and electrical conductivity studies of Mg(II), Ca(II), Sr(II) and Ba(II) vitamin B2 complexes, J. Mol. Str. 994 (2011), 194-201.

[36] S. Ilhan, H. Temel, I. Yilmaz and M. Şekerci, Synthesis and characterization of new macrocyclic Schiff base derived from 2,6-diaminopyridine and 1,7-bis(2-formylphenyl)-1,4,7-trioxaheptane and its Cu(II), Ni(II), Pb(II), Co(III) and La(III) complexes, Polyhedron 26 (2007), 2795-2802.

[37] M. Wang, L.-F. Wang, Y.-Z. Li, Q.-X. Li, Z.-D. Xu and D.-M. Qu, Antitumour activity of transition metal complexes with the thiosemicarbazone derived from 3-acetylumbelliferone, Trans. Met. Chem. 26 (2001), 307-310.

[38] G. Ibrahim, E. Chebli, M. Khan and G. Bouet, Metallic complexes from 2-furaldehyde semicarbazone and 5-methyl-(2-furaldehyde) semicarbazone, Trans. Met. Chem. 24 (1999), 294-298.

[39] A. Majumder, G. M. Rosair, A. Mallick, N. Chattopadhyay and S. Mitra, Synthesis, structures and fluorescence of nickel, zinc and cadmium complexes with the N,N,O-tridentate Schiff base N-2-pyridylmethylidene-2-hydroxy-phenylamine, Polyhedron 25 (2006), 1753-1762.

[40] S. Chandra and A. Kumar, Spectral, IR and magnetic studies of Mn(II), Co(II), Ni(II) and Cu(II) complexes with pyrrole-2-carboxyaldehyde thiosemicarbazone (L), Spectrochimica Acta Part A: Molecular and Biomolecular Spectroscopy 68 (2007), 469-473.

[41] G. G. Mohamed, M. M. Omar and A. M. M. Hindy, Synthesis, characterization and biological activity of some transition metals with Schiff base derived from 2-thiophene carboxaldehyde and aminobenzoic acid, Spectrochimica Acta Part A 62 (2005), 1140-1150.

[42] Z. H. A. El-Wahab, Mononuclear metal complexes of organic carboxylic acid derivatives: Synthesis, spectroscopic characterization, thermal investigation and antimicrobial activity, Spectrochimica Acta Part A 67 (2007), 25-38.

[43] A. M. A. El-Seidy, M. M. E. Shakdofa and H. Alshater, Synthesis and characterisation of a porphyrin like Schiff base ligand, its metal complexes and their investigation as antibacterial and antifungal agents, Journal of Applied Sciences Research 9 (2013), 2279-2286.

[44] S. R. Yaul, A. R. Yaul, G. B. Pethe and A. S. Aswar, Synthesis and characterization of transition metal complexes with N,O-Chelating hydrazone Schiff base ligands, Am.-Eura. J. Sci. Res. 4 (2009), 229-234.

[45] M. N. Patel and V. J. Patel, Studies on novel coordination polymers of a tetradentate ligand with some transition metal ions, Synthesis and Reactivity in Inorganic and Metal-Organic Chemistry 19 (1989), 137-155.

[46] S. M. Emam, F. A. El-Saie, S. A. A. El-Enein and H. A. El-Shater, Cobalt(II), nickel(II), copper(II), zinc(II) and hafnium(IV) complexes of N′-(furan-3-ylmethylene)-2-(4-methoxyphenylamino) acetohydrazide, Spectrochimica Acta Part A: Molecular and Biomolecular Spectroscopy 72 (2009), 291-297.

[47] K. Gudasi, M. Patil, R. Vadvai, R. Shenoy and S. Patil, Transition metal complexes with a new tridentate ligand, 5-6-(5-mercapto-1,3,4-oxadiazol-2-yl)pyridin-2-yl-1,3,4-oxadiazole-2-thiol, J. Serb. Chem. Soc. 72 (2007), 357-566.

[48] T. Rosu, M. Negoiu, S. Pasculescu, E. Pahontu, D. Poirier and A. Gulea, Metal-based biologically active agents: Synthesis, characterization, antibacterial and antileukemia activity evaluation of Cu(II), V(IV) and Ni(II) complexes with antipyrine-derived compounds, Eur. J. Med. Chem. 45 (2010), 774-781.

[49] S. Chandra and U. Kumar, Spectral and magnetic studies on manganese(II), cobalt(II) and nickel(II) complexes with Schiff bases, Spectrochimica Acta Part A: Molecular and Biomolecular Spectroscopy 61 (2005), 219-224.

[50] J. T. Makode, A. R. Yaul, S. G. Bhandage and A. S. Aswar, Russ. J. Coord. Chem. 54 (2009), 1372-1377.

[51] V. D. Badwaik, R. D. Deshmukh and A. S. Aswar, Synthesis, structural, and biological studies of some bivalent metal ion complexes with the tridentate Schiff base ligand, Russ. J. Coord. Chem. 35 (2009), 247-252.

[52] E. A. Elzahany, K. H. Hegab, S. K. H. Khalil and N. S. Youssef, Synthesis, characterization and biological activity of some transition metal complexes with Schiff bases derived from 2-formylindole, salicyladehyde, and N-amino rhodanine, Australian Journal of Basic and Applied Sciences 2 (2008), 210-220.

[53] K. Girish Kumar and K. Saji John, Complexation and ion removal studies of a polystyrene anchored Schiff base, Reactive and Functional Polymers 66 (2006), 1427-1433.

[54] N. Raman, S. Ravichandran and C. Thangaraja, Copper(II), cobalt(II), nickel(II) and zinc(II) complexes of Schiff base derived from benzil-2,4-dinitrophenylhydrazone with aniline, J. Chem. Sci. 116 (2004), 215-219.

[55] M. Tümer, D. Ekinci, F. Tumer and A. Bulut, Synthesis, characterization and properties of some divalent metal(II) complexes: Their electrochemical, catalytic, thermal and antimicrobial activity studies, Spectrochim. Acta Part A: Mol. Biomol. Spectrosc. 67 (2007), 916-929.

■